LASER INTERFEROMETER GRAVITATIONAL WAVE OBSERVATORY
- LIGO -
CALIFORNIA INSTITUTE OF TECHNOLOGY
MASSACHUSETTS INSTITUTE OF TECHNOLOGY

Technical Note	**LIGO-T1500461–v3**	2015/12/14

Frequency response of the aLIGO interferometer: part 2

Kiwamu Izumi, Daniel Sigg and Keita Kawabe
for the aLIGO ISC group

Distribution of this document:

LIGO VIRGO scientific collaboration, and public

California Institute of Technology
LIGO Project, MS 100-36
Pasadena, CA 91125
Phone (626) 395-2129
Fax (626) 304-9834
E-mail: info@ligo.caltech.edu

Massachusetts Institute of Technology
LIGO Project, NW22-295
Cambridge, MA 02139
Phone (617) 253-4824
Fax (617) 253-7014
E-mail: info@ligo.mit.edu

LIGO Hanford Observatory
PO Box 159
Richland, WA 99352
Phone (509) 372-8106
Fax (509) 372-8137
E-mail: info@ligo.caltech.edu

LIGO Livingston Observatory
19100 LIGO Lane
Livingston, LA 70754
Phone (225) 686-3100
Fax (225) 686-7189
E-mail: info@ligo.caltech.edu

http://www.ligo.caltech.edu/

Contents

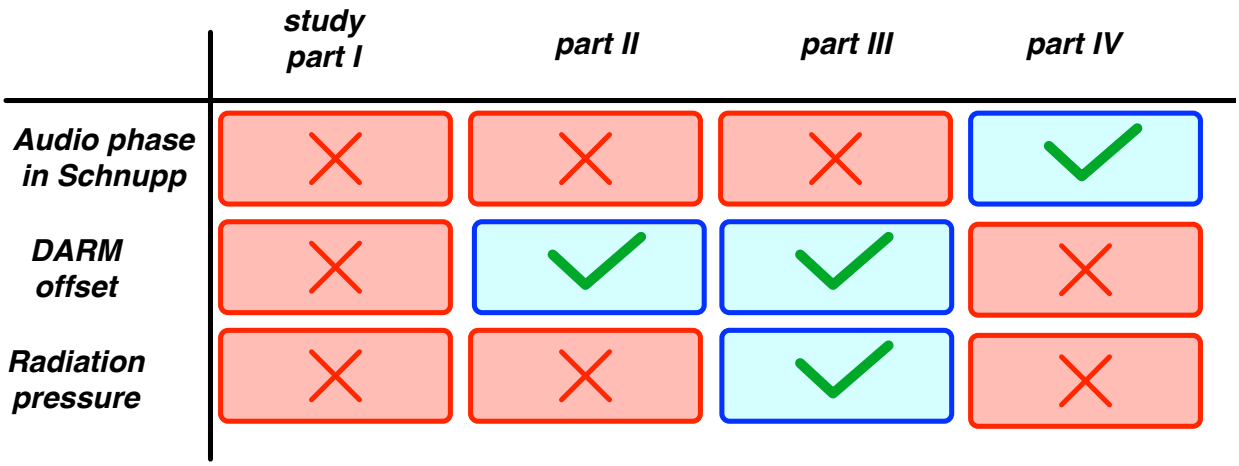

Figure 1: The (tetative) plan of the study. We plan to proceed with four steps. A red box indicates that the corresponding effect is not included while the blue boxes for the included.

1 Overview

1.1 Overview of the whole study

A goal of this study is to deliver clear and accurate picture of how we sense and control the length degrees of freedom (DOFs). For this purpose, we attempt to write down relevant interferometer responses as frequency responses in analytic form which should make underlying physics more apparent. We will intentionally start from a simple configuration and gradually add a few realistic complexities to our model as illustrated in figure 1. Throughout the study, we assume the electric fields to be plane-waves which propagate between well-aligned optics. Therefore neither mode-matching nor misalignment effects are considered.

1.2 Overview of this particular document

This document summarizes the second part of the study. As shown in figure 1, the results presented in this document are derived under the following assumptions that (1) audio sidebands in the Schnupp asymmetry do not rotate and (2) no radiation pressure effect is included. Since we now include the DARM offset, we will discuss the DC readout. In addition, we discuss the noise coupling of laser noises to the DC readout with realistic asymmetries considered.

The outline of this document is as follows. In section 2, we briefly explain how we incorporate

the DC readout. In section 3, we discuss the frequency responses at the relevant signal ports. In section 4, we discuss the coupling of laser noises to the AS port. Finally, we conclude this study in section 5 with some remarks for the next step. In addition, Appendix A provides a quick review of the definitions. Some more details of the definitions and the calculation method can be found in the first document [1].

2 Preparation for DC readout

This section describes how we handle and incorporate the DC readout and its associated DARM offset in the analytic calculations.

2.1 DARM offset

In order to perform the DC readout, we introduce an intentional offset in the DARM degree of freedom by ΔL_ϵ. We shall call ΔL_ϵ *DARM offset* hereafter. The size of the offset in one arm is identical to the other with the opposite sign. So that the individual arm length can be expressed by

$$\begin{aligned} L_x &= \frac{\lambda}{2} n + \Delta L_\epsilon, \\ L_y &= \frac{\lambda}{2} m - \Delta L_\epsilon, \end{aligned} \tag{1}$$

where n and m are integers in order for the carrier light to meet the resonance condition. According to our definition of DARM (37), it is now displaced from the resonance point by ΔL_ϵ as

$$L_- = \frac{L_x - L_y}{2} = \Delta L_\epsilon + \frac{\lambda}{2}(n+m), \tag{2}$$

while CARM does not get affected by the DARM offset.

In some cases, we refer to the DARM offset in terms of the optical distance as,

$$\epsilon = k \Delta L_\epsilon. \tag{3}$$

2.2 Handling the round trip phase in the arms

While we properly handle the round trip phase of the carrier light in a single arm in the presence of the DARM offset, we will keep approximating that of the rf sidebands to be exactly anti-resonant regardless of how big ΔL_ϵ is in the analytic calculation. A justification is given in the followings.

When a small displacement is added to an arm with the intracavity field being anti-resonant, it is going to shift the phase of the reflected field by an amount in proportion to $\hat{r_{\rm a}}' \approx T_{\rm i}/4$. Therefore the change in the reflectivity can be evaluated as,

$$\delta\hat{r_{\rm a}} = i\hat{r_{\rm a}}' \times (2k\Delta L_\epsilon) \approx i\frac{T_{\rm i}}{4} \times (2k\Delta L_\epsilon) \sim i4 \times 10^{-7} \times \left(\frac{\Delta L_\epsilon}{10\ \mathrm{pm}}\right). \tag{4}$$

Comparing this with the nominal value of $\hat{r_{\rm a}}$ which is close to 1, one can see that the DARM offset does not affect the reflection of the rf sidebands. So for the reason, we approximate the rf sidebands to be exact anti-resonance.

By the way, the same analysis for the carrier field shows that the effect is much larger.

$$\delta r_{\rm a} = ir_{\rm a}' \times (2k\Delta L_\epsilon) \sim i0.034 \left(\frac{\Delta L_\epsilon}{10\ \mathrm{pm}}\right). \tag{5}$$

So the imaginary part of the reflectivity changes almost 3% of the real part of the nominal reflectivity. As sumarized in appendix B, this is big enough to change the static fields at some parts of the interferometer while the rest are unchanged to first order.

2.3 DC readout

In this subsection, we derive a set of equations for the response of the DC readout. In general, the field at the AS port can be composed of multiple frequency components as,

$$\begin{aligned} E_{\rm AS} = {} & E_0 e^{i\omega_0 t} + E_{0u} e^{i(\omega_0+\omega)t} + E_{0l} e^{i(\omega_0-\omega)t} \\ & + E_1 e^{i(\omega_0+\omega_{\rm m})t} + E_{1u} e^{i(\omega_0+\omega_{\rm m}+\omega)t} + E_{1l} e^{i(\omega_0+\omega_{\rm m}-\omega)t} \\ & + E_{-1} e^{i(\omega_0+\omega_{\rm m})t} + E_{-1u} e^{i(\omega_0+\omega_{\rm m}+\omega)t} + E_{-1l} e^{i(\omega_0+\omega_{\rm m}-\omega)t}, \end{aligned} \tag{6}$$

where ω_0, ω and $\omega_{\rm m}$ are the laser, audio and rf frequencies respectively. We have included only one rf modulation at $\omega_{\rm m}$. Using this equation, one can find the resultant intensity at around ω to be,

$$I = 2\Re\Big[\left(E_0 E_{0l}^* + E_0^* E_{0u}\right) e^{i\omega t} + \left(E_1 E_{1l}^* + E_1^* E_{1u}\right) e^{i\omega t} + \left(E_{-1} E_{-1l}^* + E_{-1}^* E_{-1u}\right) e^{i\omega t}\Big], \tag{7}$$

where the first term represents a signal from the carrier light and the rest represent the ones from the rf sidebands.

Since it is already in the form of $S = \Re\Big[Se^{i\omega t}\Big]$, S simply represents the transfer function after all [4]. Therefore in summary, the response of the DC readout can be calculated by

$$S\left(\omega\right) = 2\left(E_0 E_{0l}^* + E_0^* E_{0u} + E_1 E_{1l}^* + E_1^* E_{1u} + E_{-1} E_{-1l}^* + E_{-1}^* E_{-1u}\right) \tag{8}$$

In some cases, it is convenient to split the response into two components – the carrier and the rf components. So that

$$\begin{aligned} S^{(\rm c)}\left(\omega\right) =& 2\left(E_0 E_{0l}^* + E_0^* E_{0u}\right), \\ S^{(\rm sb)}\left(\omega\right) =& 2\left(E_1 E_{1l}^* + E_1^* E_{1u} + E_{-1} E_{-1l}^* + E_{-1}^* E_{-1u}\right). \end{aligned} \tag{9}$$

2.4 OMC transmissivity

We assume the output mode cleaner (OMC) to be critically coupled to the carrier light without losses. Any rf sidebands are assumed to be exact anti-resonant. So that

$$\begin{aligned} T_{\rm omc}^{(\rm c)} &= 1, \\ T_{\rm omc}^{(\rm sb)} &= \left(\frac{\pi}{2\mathscr{F}}\right)^2. \end{aligned} \tag{10}$$

Here we have used equation (3.1) of [5] to express the sideband transmissivity. $\mathscr{F}$ is the OMC cavity finesse. Assuming a finesse of 390 [6], one can find $T_{\rm omc}^{(\rm sb)} = 1.6 \times 10^{-5}$ [1].

[1] As it turned out later, this approximation is too naive and therefore more realistic values will be used in part 3 [8].

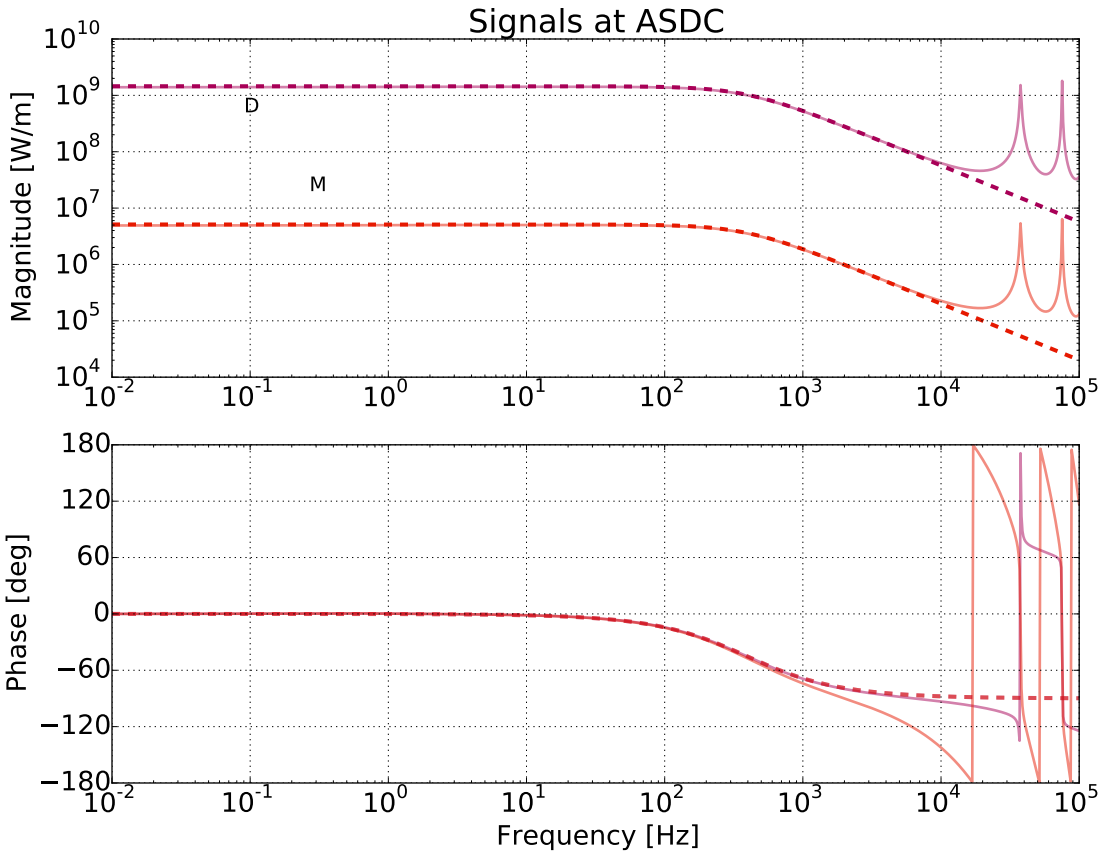

Figure 2: Frequency response at ASDC. The dashed lines represent responses derived by the approximated analytic forms, and the solid lines are the ones numerically computed without the approximations (see [1] for more detail about the approximation). The annotation letters indicate the following signals, D; DARM, M; MICH

3 Frequency responses

Following the traditional convention [3], we normalize the rf responses by $S_0 = 2J_0J_1P_{\rm in}$. Similarly, we normalize the DC readout responses by $S_1 = 2J_0^2P_{\rm in}$. We adopt the Laplace notation so that $s_{\rm c} = i\omega/\omega_{\rm c}$, $s_{\rm cc} = i\omega/\omega_{\rm cc}$ and $s_{\rm rse} = i\omega/\omega_{\rm rse}$.

3.1 AS port with DC readout

Similarly to the rf scheme, the AS port with the DC readout is sensitive to the differential modes of the interferometer. The response can be summarized as

$$\begin{aligned}\frac{S^{(\mathrm{dc})}}{S_1} =& 4g_{\mathrm{p}}^2 g_{\mathrm{s}}^2 r_{\mathrm{a}}'^2 \epsilon k \Delta L_- \frac{1}{1+s_{\mathrm{rse}}} \\ &+ 4g_{\mathrm{p}}^2 g_{\mathrm{s}}^2 r_{\mathrm{a}}' r_{\mathrm{a}} \epsilon k \Delta l_- \frac{1}{1+s_{\mathrm{rse}}}.\end{aligned} \tag{11}$$

Both DARM and MICH responses are filtered by the DARM coupled cavity pole ω_{rse} because the signals are made of purely the carrier light. As long as the upper and lower rf sidebands are balanced in their amplitudes, the rf sidebands do not contribute to the DC readout. As was the case in the rf readout, the difference in the size of the signals between DARM and MICH is a factor of $r_{\mathrm{a}}'/r_{\mathrm{a}}$. The size of both signals scales with the DARM offset so that $S^{(\mathrm{dc})} \propto \epsilon$. It is probably worthwhile to note that CARM, PRCL or SRCL do not couple to the DC readout because they excite the other quadrature of the AS field. This means that if there is contrast defect, which is on the other quadrature, then it will let CARM, PRCL and SRCL couple to the DC readout.

Here, we additionally provide a brief double check of the response at zero frequency. From equation (47), one can find the intensity at the AS port to be,

$$P_{\mathrm{AS}} = |E_{\mathrm{as}}|^2 = \left(2 g_{\mathrm{p}} g_{\mathrm{s}} r_{\mathrm{a}}' \epsilon\right)^2 .$$

Obviously the intensity behaves quadratically against a small displacement in DARM ϵ as expected. Now, taking the derivative of the intensity with respect to ϵ, one can obtain

$$\frac{\partial P_{\mathrm{AS}}}{\partial \epsilon} = 8 \left(g_{\mathrm{p}} g_{\mathrm{s}} r_{\mathrm{a}}'\right)^2 \epsilon.$$

This is consistent with the full expression shown above.

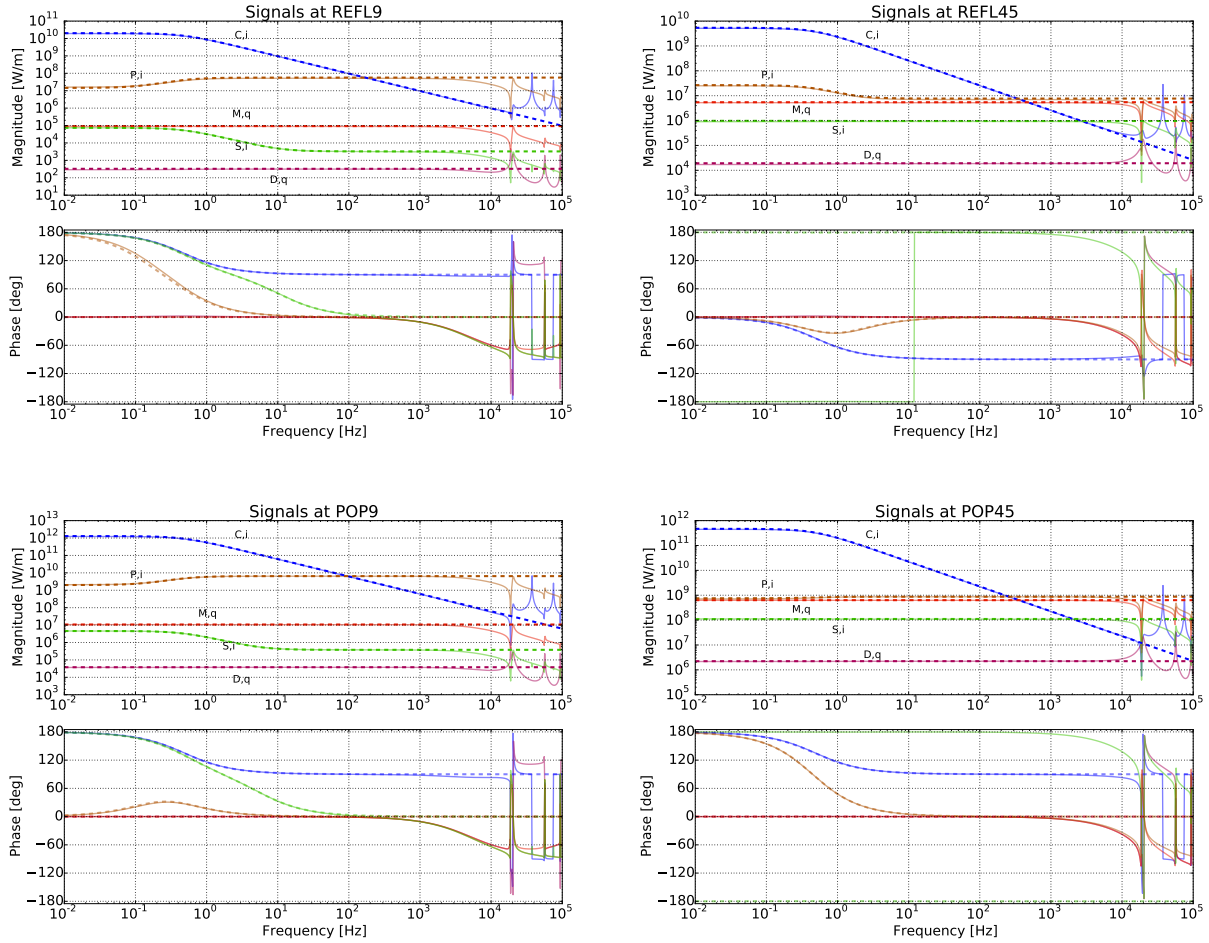

Figure 3: Frequency response at the REFL and POP ports. The dashed lines represent responses derived by the approximated analytic forms, and the solid lines are the ones numerically computed without the approximations (see [1] for more detail about the approximation). The annotation letters indicate the following signals, *C,i*; CARM in-phase, *D,q*; DARM q-phase, *M,q*; MICH q-phase, *P,i*; PRCL in-phase, *S,i*; SRCL in-phase.

3.2 REFL port

All the signals remain the same as those without the DARM offset except for SRCL. The response can be written as

$$\begin{aligned}\frac{S^{(\mathrm{refl})}}{S_0} =& -4g_{\mathrm{p}}^2 r'_{\mathrm{a}} r_{\mathrm{sb}} \frac{1}{1+s_{\mathrm{cc}}} k\Delta L_+ \cos\omega_{\mathrm{m}} t \\ &+ 4g_{\mathrm{sb}}^2 r_{\mathrm{c}} \hat{r_{\mathrm{a}}}' \chi k\Delta L_- \sin\omega_{\mathrm{m}} t \\ &- 4g_{\mathrm{sb}}^2 r_{\mathrm{c}} \hat{r_{\mathrm{a}}} \chi k\Delta l_- \sin\omega_{\mathrm{m}} t \\ &- 4\left(g_{\mathrm{p}}^2 r_{\mathrm{a}} r_{\mathrm{sb}} + g_{\mathrm{sb}}^2 r_{\mathrm{c}} r_{\mathrm{sm}}\right) \frac{1+s_{\mathrm{r}}}{1+s_{\mathrm{cc}}} k\Delta l_{\mathrm{p}} \cos\omega_{\mathrm{m}} t \\ &\mp 4\frac{\left(t_{\mathrm{c}}^2 r_{\mathrm{sb}} - g_{\mathrm{sb}}^2 r_{\mathrm{c}} t_{\mathrm{sm}}^2\right) r_{\mathrm{s}}}{t_{\mathrm{s}}^2} \frac{1+s_{\mathrm{sr}}}{1+s_{\mathrm{cc}}} k\Delta l_{\mathrm{s}} \cos\omega_{\mathrm{m}} t\end{aligned} \tag{12}$$

where

$$\chi = \frac{1 - r_{\rm s}^2 \hat{r_{\rm a}}^2}{(1 \mp r_{\rm s} r_{\rm M})^2} \sin\left(\frac{2\omega_{\rm m} l_{\rm sch}}{c}\right), \tag{13}$$

represents the coupling coefficient of the rf sideband for the differential modes to the symmetric port, and

$$t_c = 2 g_{\rm p} g_{\rm s} r'_{\rm a} \epsilon, \tag{14}$$

represents carrier's transmissivity for the whole interferometer. Also $\omega_{\rm r}$ and $\omega_{\rm sr}$ are zeros for the PRCL and SRCL responses respectively. They are defined as,

$$\begin{aligned} \omega_{\rm r} =& \omega_{\rm cc}\left(1 + \frac{g_{\rm p}^2 r_{\rm a} r_{\rm sb}}{g_{\rm sb}^2 r_{\rm c} r_{\rm sm}}\right), \\ \omega_{\rm sr} =& \omega_{\rm cc}\left(1 - \frac{t_{\rm c}^2 r_{\rm sb}}{g_{\rm sb}^2 r_{\rm c} t_{\rm sm}^2}\right). \end{aligned} \tag{15}$$

The responses are plotted in the upper panels of figure 3.

The signal recycling cavity now stores a small fraction of the carrier light due to the DARM offset. Consequently, excitation on SRC length is now able to create audio sidebands of the carrier light which then enter the power recycling cavity and therefore are filtered by the CARM cavity pole $\omega_{\rm cc}$. The addition of such a response to the existing flat response results in a pair of zero and pole in the response. This is exactly the same effect as see in the PRCL response.

The SRCL response differs between the two modulation frequencies. The response for the 9 MHz shows an easily noticeable zero-pole pair while the 45 MHz does not. This is a consequence of two facts. First, the 9 MHz sideband has a larger amount of reflection at the REFL port. This makes the carrier-audio-based signal larger for the 9 MHz. The other fact is that the audio sidebands of the 45 MHz rf sideband is sensitive to displacement in SRCL while the 9MHz is much less sensitive. This is a consequence of the resonant condition for the rf sidebands. Since the 45 MHz is set to be resonant, it produces larger audio sidebands than that of the 9 MHz. In the end, these two facts make the carrier-audio-sideband signal larger for the 9 MHz and hence the different transfer function shape as shown in the figure.

3.3 POP port

As was the case in the previous study [1], the POP port is very similar to the REFL port. The SRCL response is the only modified term due to the presence of the DARM offset. The response can be written as,

$$\begin{aligned}\frac{S^{(\mathrm{pop})}}{S_0} =& \frac{4g_{\mathrm{p}}^2 g_{\mathrm{sb}} r'_{\mathrm{a}} r_{\mathrm{sm}}}{t_{\mathrm{p}}} \frac{1}{1+s_{\mathrm{cc}}} k\Delta L_+ \cos\omega_{\mathrm{m}} t \\ &+ 4\frac{g_{\mathrm{p}} g_{\mathrm{sb}}^2 r_{\mathrm{a}} \hat{r_{\mathrm{a}}}'}{t_{\mathrm{p}}} \chi k\Delta L_- \sin\omega_{\mathrm{m}} t \\ &- 4\frac{g_{\mathrm{p}} g_{\mathrm{sb}}^2 r_{\mathrm{a}} \hat{r_{\mathrm{a}}}}{t_{\mathrm{p}}} \chi k\Delta l_- \sin\omega_{\mathrm{m}} t \\ &+ 4\left(g_{\mathrm{p}} - g_{\mathrm{sb}}\right) \frac{g_{\mathrm{p}} g_{\mathrm{sb}} r_{\mathrm{a}} r_{\mathrm{sm}}}{t_{\mathrm{p}}} \frac{1+s_{\mathrm{p}}}{1+s_{\mathrm{cc}}} k\Delta l_{\mathrm{p}} \cos\omega_{\mathrm{m}} t \\ &\pm 4\frac{g_{\mathrm{sb}} r_{\mathrm{s}} \left(r_{\mathrm{sm}} t_{\mathrm{c}}^2 + g_{\mathrm{p}} g_{\mathrm{sb}} r_{\mathrm{a}} t_{\mathrm{sm}}^2\right)}{t_{\mathrm{p}} t_{\mathrm{s}}^2} \frac{1+s_{\mathrm{sp}}}{1+s_{\mathrm{cc}}} k\Delta l_{\mathrm{s}} \cos\omega_{\mathrm{m}} t,\end{aligned} \tag{16}$$

where

$$\begin{aligned}\omega_{\mathrm{p}} =& \omega_{\mathrm{cc}} \left(1 - \frac{g_{\mathrm{p}}}{g_{\mathrm{sb}}}\right), \\ \omega_{\mathrm{sp}} =& \omega_{\mathrm{cc}} \left(1 + \frac{r_{\mathrm{sm}} t_{\mathrm{c}}^2}{g_{\mathrm{p}} g_{\mathrm{sb}} r_{\mathrm{a}} t_{\mathrm{sm}}^2}\right).\end{aligned} \tag{17}$$

The lower panels of figure 3 show the response of all the degrees of freedom.

3.4 Effect of the CARM loop

In order to simulate the effect of the CARM loop, we set the left hand side of equation (12) to be zero. Also, we drop the MICH and DARM signals because they are in the quadrature phase. This gives us the following relation,

$$\begin{aligned}4g_{\mathrm{p}}^2 r'_{\mathrm{a}} r_{\mathrm{sb}}^{(9)} \frac{1}{1+s_{\mathrm{cc}}} k\Delta L_+ =& -4\left[g_{\mathrm{p}}^2 r_{\mathrm{a}} r_{\mathrm{sb}}^{(9)} + \left(g_{\mathrm{sb}}^{(9)}\right)^2 r_{\mathrm{c}} r_{\mathrm{sm}}^{(9)}\right] \frac{1+s_{\mathrm{r}}^{(9)}}{1+s_{\mathrm{cc}}} k\Delta l_{\mathrm{p}} \\ &- 4\frac{\left[t_{\mathrm{c}}^2 r_{\mathrm{sb}}^{(9)} - \left(g_{\mathrm{sb}}^{(9)}\right)^2 r_{\mathrm{c}} \left(t_{\mathrm{sm}}^{(9)}\right)^2\right] r_{\mathrm{s}}}{t_{\mathrm{s}}^2} \frac{1+s_{\mathrm{sr}}^{(9)}}{1+s_{\mathrm{cc}}} k\Delta l_{\mathrm{s}}.\end{aligned} \tag{18}$$

where we have added the superscript "(9)" for the quantities that are associated with the 9 MHz rf sidebands. One can see that the residual CARM ΔL_+ now follows the PRCL and

SRCL residuals $\Delta l_{\rm p}$, $\Delta l_{\rm s}$. Plugging the above relation to other ports, one can obtain the modified responses.

First, let us take a look at the POP port with the 9 MHz demodulation. Plugging equation (18) to equation (16), one can find

$$\begin{aligned}\left.\frac{S^{(\mathrm{pop},\,9)}}{S_0}\right|_{\text{w/ carm}} =& -4\frac{\left(g_{\rm sb}^{(9)}\right)^2 r_{\rm sm}^{(9)}\left[g_{\rm p} r_{\rm sb}^{(9)} r_{\rm a} + g_{\rm sb}^{(9)} r_{\rm c} r_{\rm sm}^{(9)}\right]}{t_{\rm p} r_{\rm sb}^{(9)}} k\Delta l_{\rm p} \\ &+ 4\frac{\left(g_{\rm sb}^{(9)} t_{\rm sm}^{(9)}\right)^2\left[g_{\rm p} r_{\rm sb}^{(9)} r_{\rm a} + g_{\rm sb}^{(9)} r_{\rm c} r_{\rm sm}^{(9)}\right]}{t_{\rm p} t_{\rm s}^2 r_{\rm sb}^{(9)}} k\Delta l_{\rm s}.\end{aligned} \tag{19}$$

Obviously, the frequency dependencies $s_{\rm cc}$ disappeared and therefore the PRCL and SRCL responses are now flat responses.

The same analysis can be applied to that for the 45 MHz, but results in slightly complicated responses as,

$$\begin{aligned}\left.\frac{S^{(\mathrm{pop},\,45)}}{S_0}\right|_{\text{w/ carm}} =& -4\frac{g_{\rm sb}^{(45)} r_{\rm sm}^{(45)}\left[g_{\rm p} g_{\rm sb}^{(45)} r_{\rm sb}^{(9)} r_{\rm a} + \left(g_{\rm sb}^{(9)}\right)^2 r_{\rm c} r_{\rm sm}^{(9)}\right]}{t_{\rm p} r_{\rm sb}^{(9)}} k\Delta l_{\rm p} \\ &- \left\{4\frac{g_{\rm sb}^{(45)} r_{\rm s}\left[g_{\rm p} g_{\rm sb}^{(45)} r_{\rm sb}^{(9)} r_{\rm a}\left(t_{\rm sm}^{(45)}\right)^2 - \left(g_{\rm sb}^{(9)}\right)^2 r_{\rm c} r_{\rm sm}^{(45)}\left(t_{\rm sm}^{(9)}\right)^2\right]}{t_{\rm p} t_{\rm s}^2 r_{\rm sb}^{(9)}} + 8\frac{g_{\rm sb}^{(45)} r_{\rm s} r_{\rm sm}^{(45)} t_{\rm c}^2}{t_{\rm p} t_{\rm s}^2\left(1+s_{\rm cc}\right)}\right\} k\Delta l_{\rm s}\end{aligned} \tag{20}$$

As one can see, the SRCL has a frequency dependence. However, evaluating the last term in the curly brackets for SRCL, one can find it to be negligible. Therefore we can approximate the last equation to

$$\begin{aligned}\left.\frac{S^{(\mathrm{pop},\,45)}}{S_0}\right|_{\text{w/ carm}} \approx& -4\frac{g_{\rm sb}^{(45)} r_{\rm sm}^{(45)}\left[g_{\rm p} g_{\rm sb}^{(45)} r_{\rm sb}^{(9)} r_{\rm a} + \left(g_{\rm sb}^{(9)}\right)^2 r_{\rm c} r_{\rm sm}^{(9)}\right]}{t_{\rm p} r_{\rm sb}^{(9)}} k\Delta l_{\rm p} \\ &- 4\frac{g_{\rm sb}^{(45)} r_{\rm s}\left[g_{\rm p} g_{\rm sb}^{(45)} r_{\rm sb}^{(9)} r_{\rm a}\left(t_{\rm sm}^{(45)}\right)^2 - \left(g_{\rm sb}^{(9)}\right)^2 r_{\rm c} r_{\rm sm}^{(45)}\left(t_{\rm sm}^{(9)}\right)^2\right]}{t_{\rm p} t_{\rm s}^2 r_{\rm sb}^{(9)}} k\Delta l_{\rm s}.\end{aligned} \tag{21}$$

Therefore, the responses for the 45 MHz demodulation at POP are flat as well.

	$-\omega_{\rm m}$			ω_0			$+\omega_{\rm m}$		
	$-\omega_{\rm a}$	0	$+\omega_{\rm a}$	$-\omega_{\rm a}$	0	$+\omega_{\rm a}$	$-\omega_{\rm a}$	0	$+\omega_{\rm a}$
Amplitude	$iJ_1\frac{\Delta A}{2A}$	iJ_1	$iJ_1\frac{\Delta A}{2A}$	$\frac{\Delta A}{2A}$	J_0	$\frac{\Delta A}{2A}$	$iJ_1\frac{\Delta A}{2A}$	iJ_1	$iJ_1\frac{\Delta A}{2A}$
Frequency	$-iJ_1\frac{f_N}{2}$	iJ_1	$iJ_1\frac{f_N}{2}$	$-\frac{f_N}{2}$	J_0	$\frac{f_N}{2}$	$-iJ_1\frac{f_N}{2}$	iJ_1	$iJ_1\frac{f_N}{2}$
Osc Amp	$iJ_1\frac{\Delta\Gamma}{2\Gamma}$	iJ_1	$iJ_1\frac{\Delta\Gamma}{2\Gamma}$	$-\frac{\Gamma^2}{4}\frac{\Delta\Gamma}{\Gamma}$	J_0	$-\frac{\Gamma^2}{4}\frac{\Delta\Gamma}{\Gamma}$	$iJ_1\frac{\Delta\Gamma}{2\Gamma}$	iJ_1	$iJ_1\frac{\Delta\Gamma}{2\Gamma}$
Osc Phase	$J_1\frac{\Phi}{2}$	iJ_1	$J_1\frac{\Phi}{2}$	0	J_0	0	$-J_1\frac{\Phi}{2}$	iJ_1	$-J_1\frac{\Phi}{2}$

Table 1: Coefficients for all the relevant frequency components and for various noises.

Finally, we analyze the REFL port for the 45 MHz. Similarly to the 45 MHz POP, the SRCL response comes with a negligible frequency dependency and therefore one can approximate the responses as flat responses. So that,

$$\begin{aligned}\left.\frac{S^{(\text{refl, 45})}}{S_0}\right|_{\text{w/ carm}} \approx & \frac{4r_{\rm c}\left[\left(g_{\rm sb}^{(9)}\right)^2 r_{\rm sm}^{(9)} r_{\rm sb}^{(45)} - \left(g_{\rm sb}^{(45)}\right)^2 r_{\rm sm}^{(45)} r_{\rm sb}^{(9)}\right]}{r_{\rm sb}^{(9)}} k\Delta l_{\rm p} \\ & - \frac{4r_{\rm c}r_{\rm s}\left[\left(g_{\rm sb}^{(9)} t_{\rm sm}^{(9)}\right)^2 r_{\rm sb}^{(45)} + \left(g_{\rm sb}^{(45)} t_{\rm sm}^{(45)}\right)^2 r_{\rm sb}^{(9)}\right]}{r_{\rm sb}^{(9)} t_{\rm s}^2} k\Delta l_{\rm s}.\end{aligned} \tag{22}$$

4 Laser noise couplings

In this section, we introduce realistic imbalances between two arms (namely imbalance in the reflectivity and cavity pole frequency) in order to evaluate the laser noise couplings. Some details of the derivation are given in appendix C. We ignore the 9MHz rf sidebands because they reache the AS port with a small amplitude and hence a small contribution to the DC readout. Therefore we consider only the 45 MHz rf sidebands.

4.1 Arm imbalance

Besides the DARM offset, we introduce two more imbalances. The first one is the difference in the arm cavity pole frequency $\delta\omega_{\rm c}$. It is defined by

$$\delta\omega_{\rm c} = \frac{\omega_{\rm c}^{(\rm xarm)} - \omega_{\rm c}^{(\rm yarm)}}{2}. \tag{23}$$

The other one is the difference in the arm reflectivity, defined by

$$\delta r_{\rm a} = \frac{r_{\rm a}^{(\rm xarm)} - r_{\rm a}^{(\rm yarm)}}{2}. \tag{24}$$

In the numerical study, these two quantities are indirectly controlled by changing differential loss on ETMs and differential ITM tranmismittance. See table 4 for the specific values used in the numerical simulation.

4.2 Sideband expansion

Prior to the detail of the couplings, we review how we expand laser noises using the audio sidebands. We follow the convention that is described in [2, 7] with a modification in oscillator amplitude noise. A summary of the sideband expansion is give in table 1.

Amplitude noise

$$E_{\rm in} = \left(1 + \frac{\Delta A}{2A}e^{+i\omega t} + \frac{\Delta A}{2A}e^{-i\omega t}\right)\left(J_0 + iJ_1e^{+i\omega_{\rm m}t} + iJ_1e^{-i\omega_{\rm m}t}\right)E_0. \tag{25}$$

Frequency noise

$$E_{\rm in} = \left[1 + \frac{f_N}{2}\left(e^{i\omega t} - e^{-i\omega t}\right)\right]\left(J_0 + iJ_1e^{+i\omega_{\rm m}t} + iJ_1e^{-i\omega_{\rm m}t}\right)E_0, \tag{26}$$

where $f_N = \frac{2\pi\Delta f}{\omega}$.

Oscillator amplitude noise

Oscillator amplitude noise now includes the carrier modulation term which has not been taken into account in the study for iLIGO [2][7]. This inclusion revealed a higher noise coupling at low frequencies than what we have thought due to the contribution from the carrier-audio sidebands.

The input field can be expanded as

$$\begin{aligned} E_{\rm in} =& e^{i\Gamma\left(1+\frac{\Delta\Gamma}{\Gamma}\cos\omega t\right)\cos\omega_{\rm m} t} \\ \approx& J_0 - \frac{J_1\Gamma}{2}\left(\frac{\Delta\Gamma}{\Gamma}\right)\left(e^{i\omega t}+e^{-\omega t}\right) \\ &+ iJ_1\left(1+\left(\frac{\Delta\Gamma}{2\Gamma}\right)e^{i\omega t}+\left(\frac{\Delta\Gamma}{2\Gamma}\right)e^{-i\omega t}\right)\left(e^{i\omega_{\rm m} t}+e^{-i\omega_{\rm m} t}\right)+\mathcal{O}\left(\Delta\Gamma^2\right). \end{aligned} \tag{27}$$

The carrier light now has a pair of the upper and lower audio sidebands with an amplitude of $-J_1/2\Delta\Gamma$. They act as amplitude modulation sidebands around the carrier. This is intuitively correct because J_0 term is a function of Γ as $J_0 \approx 1-(\Gamma/2)^2$ and therefore the amplitude of the carrier light must be also modulated when there is a small change in Γ. If there is a small fluctuation in Γ by $\Delta\Gamma\cos\omega t$, it will produce a small deviation in J_0 as

$$(\text{small deviation in } J_0) = \frac{dJ_0}{d\Gamma}\times(\Delta\Gamma\cos\omega t) = -\frac{\Gamma\Delta\Gamma}{4}\left(e^{i\omega t}+e^{-i\omega t}\right). \tag{28}$$

This is consistent with equation (27).

Oscillator phase noise

$$E_{\rm in} = \left[J_0 + iJ_1\left[e^{i\omega_{\rm m} t}+e^{-i\omega_{\rm m} t}+i\frac{\Delta\phi}{2}\left(e^{i(\omega_{\rm m}+\omega)t}+e^{i(\omega_{\rm m}-\omega)t}-e^{i(-\omega_{\rm m}+\omega)t}-e^{i(-\omega_{\rm m}-\omega)t}\right)\right]\right]E_0. \tag{29}$$

4.3 Amplitude (or intensity) noise

Amplitude or intensity noise couples to the DC readout through two different static fields at the AS port – a field due to the DARM offset and the other due to the contrast defect. In the end, intensity noise on the DARM field beats against the static DARM field itself and

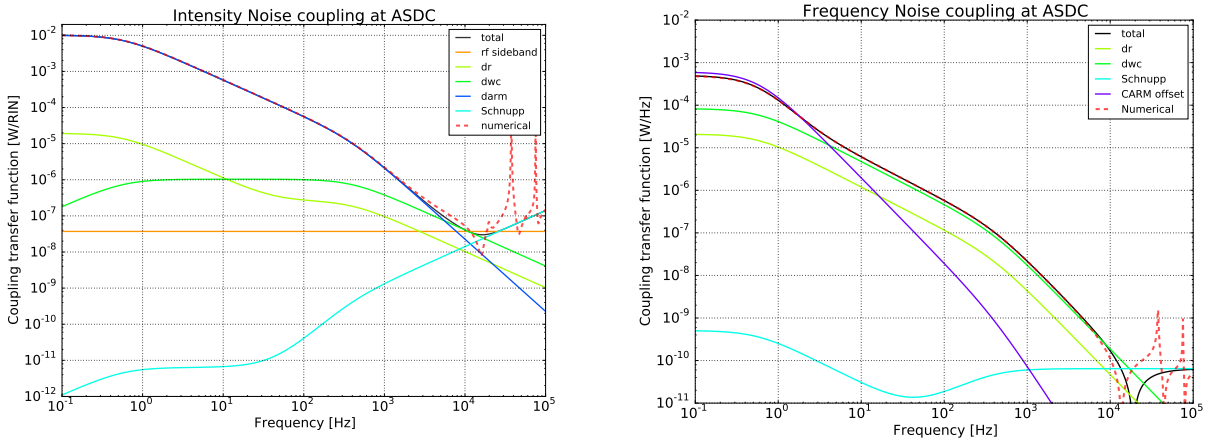

Figure 4: Intensity noise coupling (left) and frequency noise coupling (right).

creates signals. In the same fashion, intensity noise on the contrast defect beats against the static contrast defect itself and produces signals.

The coupling transfer function can be given by,

$$\begin{aligned}\frac{S^{(\mathrm{int})}}{S_1} =& \frac{\left[\left(1+r_{\mathrm{a}}\right) g_{\mathrm{p}} g_{\mathrm{s}} r'_{\mathrm{a}} \epsilon\right]^2}{\left(1+s_{cc}\right)\left(1+s_{rse}\right)} \left(\frac{\Delta A}{A}\right) \\ &+ \frac{\left(g_{\mathrm{p}} g_{\mathrm{s}}\right)^2 \delta r_{\mathrm{a}}}{\left(1+s_{cc}\right)\left(1+s_{rse}\right)} \left[\delta r_{\mathrm{a}}\left(1+s_c\right) + \frac{\delta\omega_{\mathrm{c}}}{\omega_{\mathrm{c}}} s_c \left(1+r_{\mathrm{a}}\right) - \frac{l_{\mathrm{sch}}\omega_{\mathrm{c}}}{c} r_{\mathrm{a}} s_{\mathrm{c}} \left(1 - s_c/r_{\mathrm{a}}\right)\left(1+s_c\right)\right] \left(\frac{\Delta A}{A}\right) \\ &+ 2T_{\mathrm{omc}} \left(\frac{J_1}{J_0} g_{\mathrm{sb}} t_{\mathrm{sm}}\right)^2 \left(\frac{\Delta A}{A}\right).\end{aligned} \tag{30}$$

where the first term represents intensity noise on the DARM offset field while the second term represents intensity noise imposed on the contrast defect. The last term is due to the amplitude modulation on the rf sidebands which is filtered by the OMC by the transmission coefficient T_{omc}. The response is plotted in figure 4.

The DARM coupling term is first filtered by the CARM coupled cavity pole at ω_{cc} once intensity noise enters the power recycling cavity. In addition, the propagation through the signal recycling cavity provides another filtering by the DARM coupled cavity pole ω_{rse}. The contribution from the contrast defect is also filtered by the CARM and DARM poles, but with a few extra zeros. The contrast defect term can be broken into three components as was done in the analysis for iLIGO [2, 7], namely the difference in the arm reflectivity δr_{a}, difference in the cavity pole frequency $\delta\omega_{\mathrm{c}}$ and the Schnupp asymmetry l_{sch}. As shown in

figure 4, each component couples with a different transfer function shape. The $\delta r_{\rm a}$ component shows a DC-coupled transfer function while the $\delta\omega_{\rm c}$ is AC-coupled.

4.4 Frequency noise

Although intensity noise was somewhat straightforward, frequency noise turned out to be a bit tricky because it needed to include some higher order correction when a large DARM offset exists (on the order of 10 pm). Unlike the intensity noise coupling, frequency noise on the DARM field beats against the static contrast defect. Frequency noise on the contrast defect beats against the static DARM offset. Therefore one can imagine that the resultant transfer function would be proportional to cross coupling terms of ϵ and the other asymmetries such as $\delta r_{\rm a}$, $\delta\omega_{\rm c}$ and $l_{\rm sch}$.

The response can be written as,

$$\begin{aligned}\frac{S^{(\rm freq)}}{S_1} =& \frac{2\pi\left(1+r_{\rm a}\right)\left(g_{\rm p}g_{\rm s}\right)^2 r'_{\rm a}\epsilon}{\left(1+s_{cc}\right)\left(1+s_{\rm rse}\right)}\left[-\frac{\delta r}{\omega_{\rm c}}-\frac{\delta\omega_{\rm c}}{\omega_{\rm c}^2}\left(1+r_{\rm a}\right)+\frac{l_{\rm sch}r_{\rm a}}{c}\left(1-s_c/r_{\rm a}\right)\left(1+s_c\right)\right]\Delta f \\ &+\frac{2\pi\left[\left(1+r_{\rm a}\right)g_{\rm s}\right]^2\left(g_{\rm p}r'_{\rm a}\epsilon\right)^3 Y}{\omega_{\rm cc}t_{\rm p}\left(1+s_{\rm cc}\right)^2\left(1+s_{\rm rse}\right)}\Delta f,\end{aligned} \tag{31}$$

where Y is a higher order correction term defined by

$$Y = \delta r_{\rm a}\frac{-1+2r_{\rm s}+r_{\rm a}r_{\rm s}}{1+r_{\rm a}r_{\rm s}}+\left(\frac{\delta\omega_{\rm c}}{\omega_{\rm c}}\right)\left(1+r_{\rm a}\right) \tag{32}$$

The first term in the response is the component which are transmitted through the DARM offset. As usual they are filtered by the CARM and DARM cavity poles as the light goes through to the AS port. Interestingly, both $\delta r_{\rm a}$ and $\delta\omega_{\rm c}$ have the same transfer function shape. This means that depending on the relative sign between them, their contributions can diminish (or increase) across the entire frequency band. The term associated with the Schnupp asymmetry shows an almost flat response. It usually becomes dominant at high frequencies due to the other components diminishing at high frequencies.

The last term is a dirty coupling term which scales with ϵ^3. The transfer function falls off as f^{-2} above the CARM cavity pole and keeps the f^{-2} shape until the DARM cavity pole provides another pole at $\omega_{\rm rse}$. This coupling happens because of a static phase rotation in

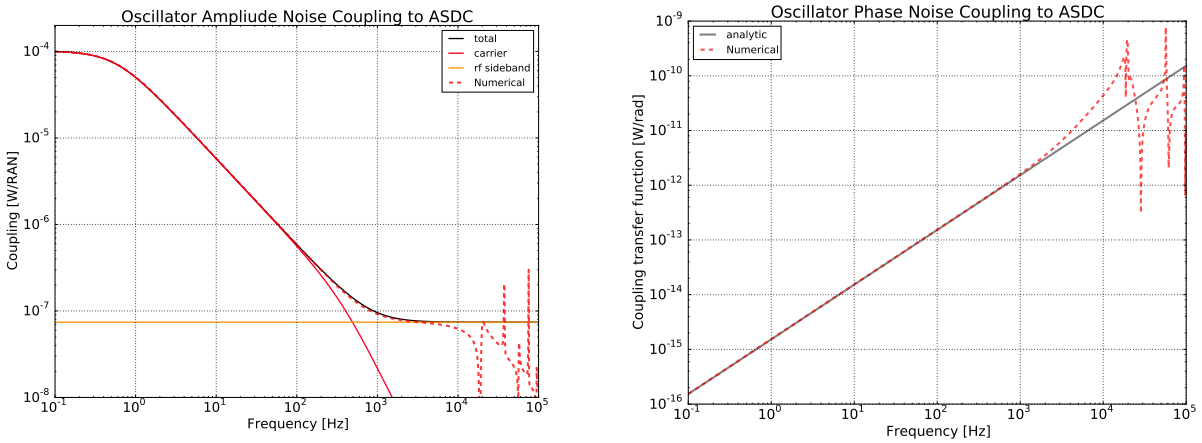

Figure 5: Oscillator amplitude noise coupling (left) and oscillator phase noise coupling (right).

the field of the power recycling cavity. The detail of this effect is discussed in appendix C.

The coupling of the rf sidebands is found to be negligible. With the parameter set provided in table 4, the coupling is found to be lower than that of the carrier light by a few orders of magnitude across the entire frequency band. Therefore we have dropped the contribution from the rf sideband.

In the next part of the study, we will show that the differential radiation pressure induced by frequency noise plays a significant role at low frequencies.

4.5 Oscillator amplitude noise coupling

The coupling of oscillator amplitude noise can be written as

$$\begin{aligned}\frac{S^{(\mathrm{osc,\,a})}}{S_1} =& -\frac{\left((1+r_\mathrm{a})\,\Gamma g_\mathrm{p} g_\mathrm{s} r'_\mathrm{a}\epsilon\right)^2}{2\,(1+s_{cc})\,(1+s_{rse})}\left(\frac{\Delta\Gamma}{\Gamma}\right)\\ &-\frac{\delta r_\mathrm{a}\left(\Gamma g_\mathrm{p} g_\mathrm{s}\right)^2}{2\,(1+s_{cc})\,(1+s_{rse})}\left[\delta r_\mathrm{a}\,(1+s_c)+\delta\omega_\mathrm{c} s_c\,(1+r_\mathrm{a})-\frac{l_\mathrm{sch}\omega_\mathrm{c}}{c}r_\mathrm{a}\,(1-s_c r_\mathrm{a})\,(1+s_c)\right]\left(\frac{\Delta\Gamma}{\Gamma}\right)\\ &+2T_\mathrm{omc}\left(\frac{J_1}{J_0}g_\mathrm{sb}t_\mathrm{sm}\right)^2\left(\frac{\Delta\Gamma}{\Gamma}\right).\end{aligned} \tag{33}$$

The first two terms are contributions from the carrier field. They are almost a copy of the carrier intensity noise coupling (30) with an extra factor of $-\Gamma^2/2$. The last term or the rf

sideband has a flat response up to a few 10 kHz and can become dominant after the carrier term drops off at high frequencies.

4.6 Oscillator phase noise coupling

The coupling transfer function was found to be,

$$\frac{S^{(\mathrm{osc,p})}}{S_1} = 2T_{\mathrm{omc}}\left(\frac{J_1}{J_0}g_{\mathrm{sb}}t_{\mathrm{sm}}\right)^2 s_c\left(\frac{l_{\mathrm{sch}}\omega_{\mathrm{c}}}{c} - \frac{2L\omega_{\mathrm{c}}}{c}\frac{\delta T_i}{T_i}\frac{\hat{r_{\mathrm{a}}}'}{\hat{r_{\mathrm{a}}}}\right)\frac{\hat{r_{\mathrm{a}}}^2 r_{\mathrm{p}} r_{\mathrm{s}}\cos\phi_{\mathrm{sch}} + \hat{r_{\mathrm{a}}}\left(r_{\mathrm{p}}+r_{\mathrm{s}}\right) + \cos\phi_{\mathrm{sch}}}{\left(1+\hat{r_{\mathrm{a}}}\left(r_{\mathrm{p}}+r_{\mathrm{s}}\right)\cos\phi_{\mathrm{sch}} + \hat{r_{\mathrm{a}}}^2 r_{\mathrm{p}} r_{\mathrm{s}}\right)\sin\phi_{\mathrm{sch}}}\Delta\phi. \tag{34}$$

As seen in figure 5, it has f-shape up to a few kHz and it scales with the Schnupp asymmetry l_{sch}.

There is an interesting effect[2]. A mismatch in the reflectivity between two ITMs δT_i changes the scaling factor of the coupling transfer function. This occurs essentially because the arm cavities act as an extra Schnupp asymmetry. The reflectivity of an arm cavity with the light anti-resonant can be written as

$$r_{\mathrm{arm}}^{(\mathrm{sb})} = \hat{r_{\mathrm{a}}} + 2i\hat{r_{\mathrm{a}}}'\frac{\omega L}{c} \tag{35}$$

where we have ignored the DARM offset. When the ITMs have a differential transmissivity mismatch, it is going to be modified as

$$r_{\mathrm{arm}}^{(\mathrm{sb})} = \hat{r_{\mathrm{a}}} + 2i\hat{r_{\mathrm{a}}}'\left[1+\left(\frac{\delta T_i}{T_i}\right)\right]\frac{\omega L}{c} \tag{36}$$

where we have ignored the small deviation in the reflection at DC and keep it unchanged as $\hat{r_{\mathrm{a}}}$. This phase rotation due to δT_{i} acts as an additional time-delay and therefore effectively expands (or shrinks) the Schnupp asymmetry.

[2] As it turned out later, this term is no longer a dominant term with the presence of the radiation pressure effect and rigorous resonance condition of the rf sidebands in the arms. Therefore we will neglect this term in part 3 [8].

5 Conclusions and prospects

We have derived a set of analytic equations that describe the frequency responses of the aLIGO interferometer to all five interferometric degrees of freedom with the DC readout incorporated. In order to introduce the DC readout we have added an offset in the DARM degree of freedom which changed the response of SRCL at the REFL and POP ports due to the signal recycling cavity becoming able to excite the carrier field. The rest of the responses were found to be unchanged with the DARM offset.

We have calculated various laser noise couplings with realistic imbalance introduced in the arm cavities. This time, we have discovered that oscillator amplitude noise creates a pair of audio sidebands not only on the rf sidebands but also the carrier field. The inclusion of the carrier light in oscillator amplitude noise significantly changes the low frequency part of the coupling transfer function due to the carrier-audio sidebands. We also confirmed that the analytic expressions that we had derived can accurately produce noise coupling transfer functions.

In the next part of the study, we will incorporate the radiation pressure effects. It is going to add another noise coupling path to laser noises and therefore will impact on the low frequency part. Also the radiation pressure will make a new coupling path for PRCL and SRCL to the AS DC readout.

CARM	$dE^{(c)} \otimes E^{(sb)}$	$E^{(c)} \otimes dE^{(sb)}$	**leading term**
REFL 9I	∃	∃	$dE^{(c)} \otimes E^{(sb)}$
REFL 9Q	-	-	-
REFL 45I	∃	∃	$dE^{(c)} \otimes E^{(sb)}$
REFL 45Q	-	-	-
POP 9I	∃	∃	$dE^{(c)} \otimes E^{(sb)}$
POP 9Q	-	-	-
POP 45I	∃	∃	$dE^{(c)} \otimes E^{(sb)}$
POP 45Q	-	-	-
AS 9I	-	-	-
AS 9Q	-	-	-
AS 45I	-	-	-
AS 45Q	-	-	-
DARM	$dE^{(c)} \otimes E^{(sb)}$	$E^{(c)} \otimes dE^{(sb)}$	**leading term**
REFL 9I	-	-	-
REFL 9Q	-	∃	$E^{(c)} \otimes dE^{(sb)}$
REFL 45I	-	-	-
REFL 45Q	-	∃	$E^{(c)} \otimes dE^{(sb)}$
POP 9I	-	-	-
POP 9Q	-	∃	$E^{(c)} \otimes dE^{(sb)}$
POP 45I	-	-	-
POP 45Q	-	∃	$E^{(c)} \otimes dE^{(sb)}$
AS 9I	-	-	-
AS 9Q	∃	-	$dE^{(c)} \otimes E^{(sb)}$
AS 45I	-	-	-
AS 45Q	∃	-	$dE^{(c)} \otimes E^{(sb)}$
MICH	$dE^{(c)} \otimes E^{(sb)}$	$E^{(c)} \otimes dE^{(sb)}$	**leading term**
REFL 9I	-	-	-
REFL 9Q	-	∃	$E^{(c)} \otimes dE^{(sb)}$
REFL 45I	-	-	-
REFL 45Q	-	∃	$E^{(c)} \otimes dE^{(sb)}$
POP 9I	-	-	-
POP 9Q	-	∃	$E^{(c)} \otimes dE^{(sb)}$
POP 45I	-	-	-
POP 45Q	-	∃	$E^{(c)} \otimes dE^{(sb)}$
AS 9I	-	-	-
AS 9Q	∃	-	$dE^{(c)} \otimes E^{(sb)}$
AS 45I	-	-	-
AS 45Q	∃	-	$dE^{(c)} \otimes E^{(sb)}$

PRCL			
	$dE^{(c)} \otimes E^{(sb)}$	$E^{(c)} \otimes dE^{(sb)}$	**leading term**
REFL 9I	∃	∃	both
REFL 9Q	-	-	-
REFL 45I	∃	∃	both
REFL 45Q	-	-	-
POP 9I	∃	∃	both
POP 9Q	-	-	-
POP 45I	∃	∃	both
POP 45Q	-	-	-
AS 9I	-	-	-
AS 9Q	-	-	-
AS 45I	-	-	-
AS 45Q	-	-	-
SRCL			
REFL 9I	∃	∃	depends on DARM offset
REFL 9Q	-	-	-
REFL 45I	∃	∃	mostly $E^{(c)} \otimes dE^{(sb)}$
REFL 45Q	-	-	-
POP 9I	∃	∃	depends on DARM offset
POP 9Q	-	-	-
POP 45I	∃	∃	mostly $E^{(c)} \otimes dE^{(sb)}$
POP 45Q	-	-	-
AS 9I	-	-	-
AS 9Q	-	-	-
AS 45I	-	-	-
AS 45Q	-	-	-

Table 2: Summary of all the responses. The elements filled with ∃ means that they have non-zero values. The elements filled with ∃ indicate that they did not exist when no DARM offset was applied. Otherwise zero signals.

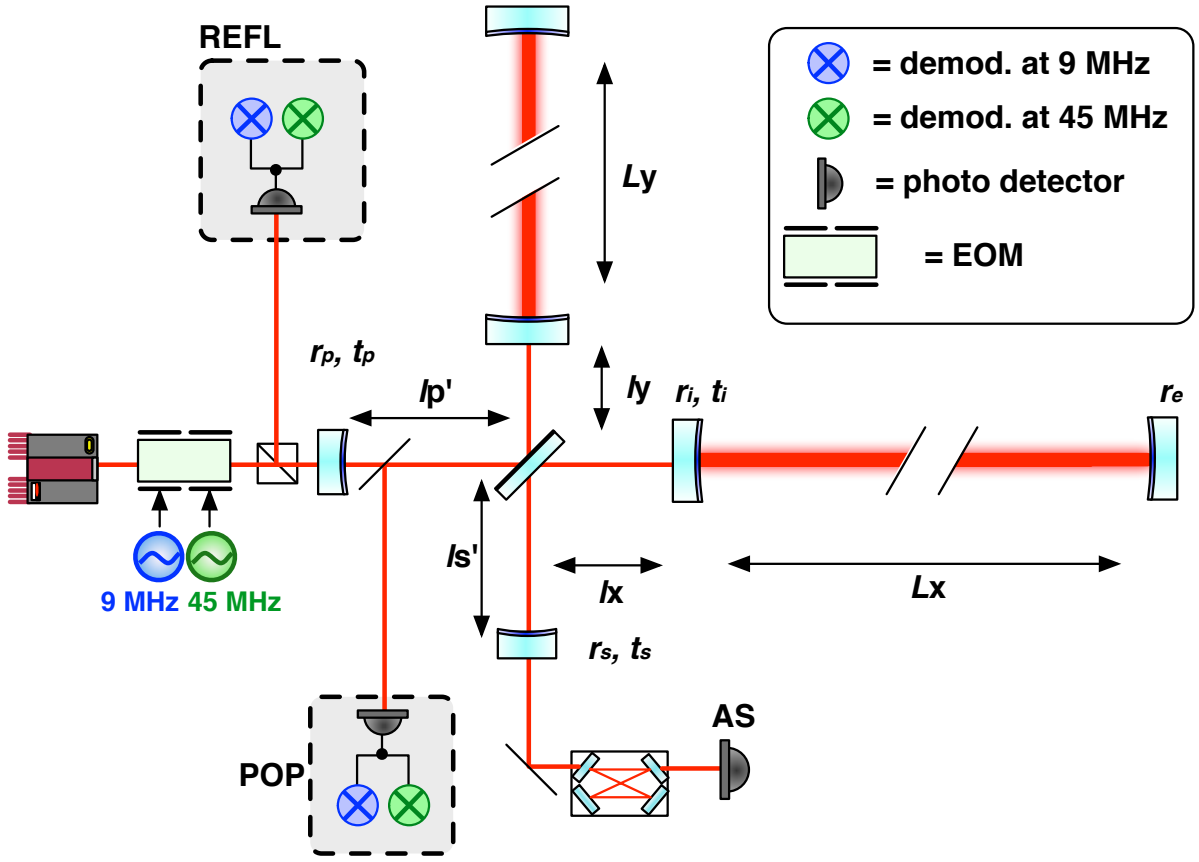

Figure 6: A schematic of the aLIGO interferometer setup.

A Definitions and setup

A.1 Length degrees of freedom

We define the length DOFs as follows,

$$\begin{aligned}
\textbf{DARM: } L_- &= \frac{L_x - L_y}{2}, \\
\textbf{CARM: } L_+ &= \frac{L_x + L_y}{2}, \\
\textbf{PRCL: } l_\mathrm{p} &= l'_p + \frac{l_x + l_y}{2}, \\
\textbf{MICH: } l_- &= \frac{l_x - l_y}{2}, \\
\textbf{SRCL: } l_\mathrm{s} &= l'_s + \frac{l_x + l_y}{2}.
\end{aligned} \tag{37}$$

The optical distances are graphically shown in figure 6.

A.2 Interferometric properties

The followings are definitions of some important quantities. For more details, see the previous document [1].

A.2.1 Quantities related to arm cavity

$$r_{\rm a} \equiv \frac{r_{\rm e}\left(t_{\rm i}^2 + r_{\rm i}^2\right) - r_{\rm i}}{1 - r_{\rm i} r_{\rm e}}, \quad \hat{r_{\rm a}} \equiv -\frac{r_{\rm e}\left(t_{\rm i}^2 + r_{\rm i}^2\right) + r_{\rm i}}{1 + r_{\rm i} r_{\rm e}}, \tag{38}$$

$$r'_{\rm a} = \frac{t_{\rm i}^2 r_{\rm e}}{\left(1 - r_{\rm i} r_{\rm e}\right)^2}, \quad \hat{r_{\rm a}}' = \frac{t_{\rm i}^2 r_{\rm e}}{\left(1 + r_{\rm i} r_{\rm e}\right)^2}, \tag{39}$$

A.2.2 Quantities related to Michelson and signal recycled Michelson

$$\begin{gathered} r_{\rm M}\left(\omega_{\rm m}\right) = \hat{r_{\rm a}} \cos\left(2\frac{\omega_{\rm m} l_{\rm sch}}{c}\right), \quad t_{\rm M}\left(\omega_{\rm m}\right) = \hat{r_{\rm a}} \sin\left(2\frac{\omega_{\rm m} l_{\rm sch}}{c}\right), \\ r_{\rm sm} = \frac{r_{\rm M} \mp \hat{r_{\rm a}}^2 r_{\rm s}}{1 \mp r_{\rm s} r_{\rm M}}, \quad t_{\rm sm} = \frac{t_{\rm s} t_{\rm M}}{1 \mp r_{\rm s} r_{\rm M}}, \end{gathered} \tag{40}$$

The upper component of the $\pm$ and $\mp$ symbols in the equations represent that for the 9 MHz rf sideband while the lower components are for the 45 MHz rf sideband.

A.2.3 Interferometer reflectivity

$$r_{\rm c} = \frac{\left(r_{\rm p}^2 + t_{\rm p}^2\right) r_{\rm a} - r_{\rm p}}{1 - r_{\rm p} r_{\rm a}}, \quad r_{\rm sb} = -\frac{\left(r_{\rm p}^2 + t_{\rm p}^2\right) r_{\rm sm} + r_{\rm p}}{1 + r_{\rm p} r_{\rm sm}}. \tag{41}$$

A.2.4 Recycling gains

$$g_{\rm p} = \frac{t_{\rm p}}{1 - r_{\rm p} r_{\rm a}}, \quad g_{\rm s} = \frac{t_{\rm s}}{1 + r_{\rm s} r_{\rm a}}, \quad g_{\rm sb} = \frac{t_{\rm p}}{1 + r_{\rm p} r_{\rm sm}}. \tag{42}$$

B Various static fields with the DARM offset

The followings are the static fields at various points of the interferometer in order to show how strongly or weakly the DARM offset affects them. As discussed in section 2, we consider the rf sideband to be unchanged and therefore we don't show them.

REFL

$$r_{\mathrm{c}}^{(\mathrm{c})} \approx r_{\mathrm{c}} + \mathcal{O}\left(\epsilon^2\right) \tag{43}$$

PRC intra fields (leaving PRM toward BS)

$$E_{\mathrm{p}}^{(\mathrm{c})} \approx g_{\mathrm{p}} E_{\mathrm{in}} + \mathcal{O}\left(\epsilon^2\right) \tag{44}$$

POP field (leaving BS toward PRM)

$$E_{\mathrm{pop}}^{(\mathrm{c})} \approx g_{\mathrm{p}} r_{\mathrm{a}} E_{\mathrm{in}} + \mathcal{O}\left(\epsilon^2\right) \tag{45}$$

SRC intra fields (leaving BS towards SRM)

$$E_{\mathrm{s}}^{(\mathrm{c})} \approx \frac{2 g_{\mathrm{p}} g_{\mathrm{s}} r'_{\mathrm{a}}}{t_{\mathrm{s}}} \epsilon E_{\mathrm{in}} + \mathcal{O}\left(\epsilon^3\right) \tag{46}$$

AS port

$$E_{\mathrm{as}}^{(\mathrm{c})} \approx 2 i g_{\mathrm{p}} g_{\mathrm{s}} r'_{\mathrm{a}} \epsilon E_{\mathrm{in}} + \mathcal{O}\left(\epsilon^3\right) \tag{47}$$

ITMs forward propagation (leaving BS toward ITMs)

$$\begin{aligned} E_{\mathrm{itmx}}^{(\mathrm{c})} &\approx \frac{g_{\mathrm{p}}}{\sqrt{2}} E_{\mathrm{in}} + i\sqrt{2} \frac{r'_{\mathrm{a}} g_{\mathrm{p}} g_{\mathrm{s}} r_{\mathrm{s}}}{t_{\mathrm{s}}} \epsilon E_{\mathrm{in}} + \mathcal{O}\left(\epsilon^2\right) \\ E_{\mathrm{itmy}}^{(\mathrm{c})} &\approx \frac{g_{\mathrm{p}}}{\sqrt{2}} E_{\mathrm{in}} - i\sqrt{2} \frac{r'_{\mathrm{a}} g_{\mathrm{p}} g_{\mathrm{s}} r_{\mathrm{s}}}{t_{\mathrm{s}}} \epsilon E_{\mathrm{in}} + \mathcal{O}\left(\epsilon^2\right) \end{aligned} \tag{48}$$

ITMs backward propagation (leaving ITMs toward BS)

$$\begin{aligned} E^{(\mathrm{c})}_{\mathrm{itmx}} &\approx \frac{g_{\mathrm{p}} r_{\mathrm{a}}}{\sqrt{2}} E_{\mathrm{in}} - i\sqrt{2}\frac{r'_{\mathrm{a}} g_{\mathrm{p}} g_{\mathrm{s}}}{t_{\mathrm{s}}}\epsilon E_{\mathrm{in}} + \mathcal{O}\left(\epsilon^2\right) \\ E^{(\mathrm{c})}_{\mathrm{itmy}} &\approx \frac{g_{\mathrm{p}} r_{\mathrm{a}}}{\sqrt{2}} E_{\mathrm{in}} + i\sqrt{2}\frac{r'_{\mathrm{a}} g_{\mathrm{p}} g_{\mathrm{s}}}{t_{\mathrm{s}}}\epsilon E_{\mathrm{in}} + \mathcal{O}\left(\epsilon^2\right) \end{aligned} \tag{49}$$

ETMs (incident on ETMs)

They are fields incident on the ETMs.

$$\begin{aligned} E^{(\mathrm{c})}_{\mathrm{etmx}} &\approx \frac{g_{\mathrm{p}} g_{\mathrm{a}}}{\sqrt{2}} E_{\mathrm{in}} - i\sqrt{2}\left(1 - r_{\mathrm{i}} r_{\mathrm{s}}\right)\frac{r'_{\mathrm{a}} g_{\mathrm{p}} g_{\mathrm{s}}}{r_{\mathrm{e}} t_{\mathrm{i}} t_{\mathrm{s}}}\epsilon E_{\mathrm{in}} + \mathcal{O}\left(\epsilon^2\right) \\ E^{(\mathrm{c})}_{\mathrm{etmy}} &\approx \frac{g_{\mathrm{p}} g_{\mathrm{a}}}{\sqrt{2}} E_{\mathrm{in}} + i\sqrt{2}\left(1 - r_{\mathrm{i}} r_{\mathrm{s}}\right)\frac{r'_{\mathrm{a}} g_{\mathrm{p}} g_{\mathrm{s}}}{r_{\mathrm{e}} t_{\mathrm{i}} t_{\mathrm{s}}}\epsilon E_{\mathrm{in}} + \mathcal{O}\left(\epsilon^2\right) \end{aligned} \tag{50}$$

C Details of laser noise couplings

We derive a set of the necessary propagation functions of laser noises to the AS port. For convenience, we split the derivation into that of the carrier light and the rf sideband. We will discuss the carrier at first and move onto the rf sidebands. The derivation for the carrier is further divided into thee pieces — The Michelson interferometer with the arm cavities, field in the power recycling cavity and propagation from the power recycling cavity to the AS port. Combining all three pieces in the end will then give us a full propagation equation.

C.1 Arm cavities and Michelson for the carrier

In this subsection, as a preparation for the later calculation, we review how we handle the arm cavities and Michelson. As usual [7, 2], we simplify the arm reflection using the following approximated form,

$$r^{(\mathrm{c})}_{\mathrm{arm}}\left(\omega; r_{\mathrm{a}}, \omega_{\mathrm{c}}, \epsilon\right) = r_{\mathrm{a}} \frac{1 - s_{\mathrm{c}}/r_{\mathrm{a}} - i r'_{\mathrm{a}}\epsilon/r_{\mathrm{a}}}{1 + s_{\mathrm{c}} + i r'_{\mathrm{a}}\epsilon}. \tag{51}$$

For the later use, we define the common and differential reflectivity of the arms as,

$$\begin{aligned} r_{\mathrm{comm}} &= \frac{r_{\mathrm{arm}}\left(\omega; r_{\mathrm{a}} + \delta r_{\mathrm{a}}, \omega_{\mathrm{c}} + \delta\omega_{\mathrm{c}}, \epsilon\right) + r_{\mathrm{arm}}\left(\omega; r_{\mathrm{a}} - \delta r_{\mathrm{a}}, \omega_{\mathrm{c}} - \delta\omega_{\mathrm{c}}, -\epsilon\right)}{2} \\ &= r^{(\mathrm{c})}_{\mathrm{arm}}\left(\omega; r_{\mathrm{a}}, \omega_{\mathrm{c}}, 0\right) - i\frac{r'_{\mathrm{a}}\epsilon}{\left(1 + s_c\right)^3}\left[dr\left(1 + s_{\mathrm{c}}\right) - \left(1 + r_{\mathrm{a}}\right)\left(1 - s_{\mathrm{c}}\right)\right], \end{aligned} \tag{52}$$

$$\begin{aligned} r_{\mathrm{diff}} &= \frac{r_{\mathrm{arm}}\left(\omega; r_{\mathrm{a}} + \delta r_{\mathrm{a}}, \omega_{\mathrm{c}} + \delta\omega_{\mathrm{c}}, \epsilon\right) - r_{\mathrm{arm}}\left(\omega; r_{\mathrm{a}} - \delta r_{\mathrm{a}}, \omega_{\mathrm{c}} - \delta\omega_{\mathrm{c}}, -\epsilon\right)}{2} \\ &\approx \frac{\delta r_{\mathrm{a}}}{1 + s_{\mathrm{c}}} + \left(\frac{\delta\omega_{\mathrm{c}}}{\omega_{\mathrm{c}}}\right)\frac{s_{\mathrm{c}}\left(1 + r_{\mathrm{a}}\right)}{\left(1 + s_{\mathrm{c}}\right)^2} - i r'_{\mathrm{a}}\epsilon\frac{1 + r_{\mathrm{a}}}{\left(1 + s_{\mathrm{c}}\right)^2} \end{aligned} \tag{53}$$

Now, moving on to the Michelson reflection and transmissivity, one can find them to be

$$\begin{aligned} r^{(\mathrm{c})}_{\mathrm{M}} &= r_{\mathrm{com}}\cos\left(\frac{\omega l_{\mathrm{sch}}}{c}\right) - i r_{\mathrm{diff}}\sin\left(\frac{\omega l_{\mathrm{sch}}}{c}\right), \\ t^{(\mathrm{c})}_{\mathrm{M}} &= i r_{\mathrm{com}}\sin\left(\frac{\omega l_{\mathrm{sch}}}{c}\right) - r_{\mathrm{diff}}\cos\left(\frac{\omega l_{\mathrm{sch}}}{c}\right). \end{aligned} \tag{54}$$

In order to differentiate those for the rf sidebands, we put a "c" superscript.

C.2 Propagation of the carrier from PRC to the AS port

We now derive the propagation function from the power recycling cavity to the AS port. Assuming the single trip phase in the signal recycling cavity is small compared with that of the arm cavities and therefore negligile, one can write the propagation transfer function as,

$$\frac{E_{\rm as}}{E_{\rm p}} = \frac{t_{\rm M}^{(\rm c)} t_{\rm s}}{1 + r_{\rm M}^{(\rm c)} r_{\rm s}} \tag{55}$$

Plugging equations (63), (52) and (53), one can obtain

$$\frac{E_{\rm as}}{E_{\rm p}} = \frac{g_{\rm s}}{1+s_{\rm rse}} \left[\frac{s_{\rm c} r_{\rm a} \omega_{\rm c} l_{\rm sch}}{c} \left(1 - s_{\rm c}/r_{\rm a}\right) - \delta r_{\rm a} - s_{\rm c} \left(\frac{\delta\omega_{\rm c}}{\omega_{\rm c}}\right) \frac{1+r_{\rm a}}{1+s_{\rm c}} + i\epsilon \frac{r'_{\rm a}\left(1+r_{\rm a}\right)}{1+s_{\rm c}} \right]. \tag{56}$$

The first term is associated wtth the Schnupp asymmetry, the second term is due to the difference in arms' reflectivity, the third term is that from the difference in arms' cavity pole frequency $\delta\omega_{\rm c}$ and the last term is the signal field provided by the DARM offset ϵ. As expected, all of them are filtered by the DARM coupled cavity pole, $\omega_{\rm rse}$ with an amplification factor of $g_{\rm s}$.

C.3 The carrier field in the power recycling cavity

Using the Michelson reflectivity $r_{\rm M}^{(\rm c)}$ and transmissivity $t_{\rm M}^{(\rm c)}$, one can write the power recycling cavity filed as

$$\frac{E_{\rm p}}{E_{\rm in}} = \frac{r_{\rm M}^{(\rm c)} + \left(r_{\rm M}^{(\rm c)} - t_{\rm M}^{(\rm c)}\right)}{1 + r_{\rm M}^{(\rm c)} r_{\rm s}}, \tag{57}$$

where we have approximated the single trip phase of the power recycling cavity to be $e^{-i\phi_{\rm prc}} \approx 1$. Now, expanding equations (63) to first order with respect to $\omega l_{\rm sch}/c \sim 0$ and plugging them to the above, one can rewrite the above expression as,

$$\frac{E_{\rm p}}{E_{\rm in}} = g_{\rm p} \frac{1+s_{\rm c}}{1+s_{\rm cc}} + i \frac{g_{\rm p}^2 r_{\rm p} r'_{\rm a} \epsilon}{t_{\rm p}\left(1+s_{\rm cc}\right)^2} Y \tag{58}$$

where Y is a frequency-independent factor which is made of two imbalances,

$$Y = \delta r_{\rm a} \frac{-1 + 2r_{\rm s} + r_{\rm a} r_{\rm s}}{1 + r_{\rm a} r_{\rm s}} + \left(\frac{\delta\omega_{\rm c}}{\omega_{\rm c}}\right)\left(1 + r_{\rm a}\right) \tag{59}$$

As shown in the above expressions, now the carrier field in the power recycling cavity has an extra phase shift in proportion to ϵY. For instance, when the carrier light is considered with $\omega = 0$, it gives us $E_{\rm p}/E_{\rm in} = g_{\rm p} + ig_{\rm p}^2 r_{\rm p} r'_{\rm a} \epsilon Y/t_{\rm p}$ where the second term is a phase shift because it comes with a complex i. As discussed in section 4.4, this extra phase then causes an extra noise coupling for frequency noise.

C.4 Full propagation from input to the AS port

Combining equations (56) and (58), one can obtain the full propagation of the carrier as,

$$\begin{aligned}\frac{E_{\rm as}}{E_{\rm in}} =& \frac{E_{\rm p}}{E_{\rm in}} \times \frac{E_{\rm as}}{E_{\rm p}} \\ =& \frac{g_{\rm p} g_{\rm s}}{(1+s_{\rm cc})(1+s_{\rm rse})}\left[\frac{\omega_{\rm c} l_{\rm sch} r_{\rm a}}{c} s_{\rm c}(1 - s_{\rm c}/r_{\rm a})(1+s_{\rm c}) - \delta r_{\rm a}(1+s_{\rm c}) - (1+r_{\rm a})\frac{\delta\omega_{\rm c}}{\omega_{\rm c}} s_{\rm c} + \right. \\ & \left. i r'_{\rm a}(1+r_{\rm a})\epsilon\right] - \frac{g_{\rm p}^2 g_{\rm s} r_{\rm p} (r'_{\rm a}\epsilon)^2 (1+r_{\rm a})}{t_{\rm p}(1+s_{\rm rse})(1+s_{\rm cc})^2(1+s_{\rm c})} Y\end{aligned} \tag{60}$$

where we have dropped the small terms that are proportional to $\delta r_{\rm a} Y$, $l_{\rm sch} Y$ and $\delta\omega_{\rm c} Y$.

Since this equation is very important, let us take a moment to think about what this expression means. First of all, notice that all the fields are filtered by the CARM and DARM coupled cavity poles with an amplification coefficient of $g_{\rm p} g_{\rm s}$ as expected. Next, the AS field is composed of two kinds of fields, the one with an imaginary i and another without an imaginary i. For example, the field related to the DARM offset ϵ is the only one which comes with an i. We can interpret this as a field in the *phase quadrature*. In contrast, the rest of the terms come without an i. This means that they are in the *amplitude quadrature* or perhaps one can say *contrast defect* fields because they do not contribute to the DARM signal but adds noises. Technically speaking, the contrast defect light affects the way we readout the signal through the homodyn angle, but it is out of scope of this document.

Next, let us take a look at each term. The first term coming with $l_{\rm sch}$ represents the field that leaks to the AS port due to the Schnupp asymmetry. Since the Michelson interferometer is locked at a dark fringe, the DC carrier light with $\omega = 0$ does not transmits to the AS port. The second term with $\delta r_{\rm a}$ is a contrast defect field that leaks to the AS port because of the imbalanced arms' reflectivity. Similarly to the $\delta r_{\rm a}$ term, the third term with $\delta\omega_{\rm c}$ is the filed

that is due to the difference in arms' cavity pole frequency. Since the cavity pole affects the size of the leakage field from each arm cavity, it is suppressed at DC. As it goes to high frequencies, the effect becomes more prominent and it is going to have the same transfer function shape as that of the $\delta r_{\rm a}$ above the cavity pole $\omega_{\rm c}$. The fourth term is a field that is provided by the DARM offset ϵ. The main purpose of this field is that this acts as a reference field for the DC readout in the context of homodyne readout. A big advantage of providing the reference field with the physical DARM offset against providing a pick-off sample of the input field is that the field is filtered by the interferometer itself with the CARM and DARM cavity poles. Therefore the reference can be more stable. The last term with Y is a field that is caused by a CARM offset. As shown in equation (58), this field originates with a phase offset in the power recycling cavity or CAMR offset. The amplitude of this field may be small, but it was found to be non-negligible when deriving frequency noise coupling (see section 4.4).

As a boule check, one can take the low frequency limit, so that

$$\left.\frac{E_{\rm as}}{E_{\rm in}}\right|_{\omega=0} = g_{\rm p} g_{\rm s} \left(2ir'_{\rm a}\epsilon - \delta r_{\rm a}\right), \tag{61}$$

where we have approximated the coefficient $(1+r_{\rm a})$ to be 2 for simplicity. This is consistent with equation 47 except that it now has a contrast defect due to $\delta r_{\rm a}$.

C.5 Double check with that of iLIGO

One can check the consistency of the above equation (60), by setting $t_{\rm s} \to 1$ and $r_{\rm s} \to 0$ and comparing with that for iLIGO. This forces us to drop the signal recycling gain so that $g_{\rm s} \to 1$. Also, the DARM cavity pole is now shifted back to that for a single arm cavity so that $\omega_{\rm rse} \to \omega_{\rm c}$. After all, equation (60) can be reduced to

$$\begin{aligned}\left.\frac{E_{\rm as}}{E_{\rm in}}\right|_{\text{no SRM}} =& \frac{g_{\rm p}\omega_{\rm c} l_{\rm sch} r_{\rm a}}{c} \frac{s_{\rm c}\left(1 - s_{\rm c}/r_{\rm a}\right)}{1+s_{\rm cc}} \\ &- \left(\frac{\delta\omega_{\rm c}}{\omega_{\rm c}}\right) \frac{g_{\rm p} s_{\rm c}\left(1+r_{\rm a}\right)}{\left(1+s_{\rm cc}\right)\left(1+s_{\rm c}\right)} - \frac{g_{\rm p}\delta r_{\rm a}}{1+s_{\rm cc}} + \frac{2ig_{\rm p} r'_{\rm a} k\epsilon}{\left(1+s_{\rm cc}\right)\left(1+s_{\rm c}\right)}.\end{aligned} \tag{62}$$

We have dropped the CARM offset term by setting $\epsilon^2 Y \to 0$. Paying attention to the fact that Sigg (1997) [2] uses different parameter definitions,

$$l_{\rm sch} \to \frac{1}{2} l_{\rm sch}, \quad \delta\omega \to \frac{1}{2}\delta\omega, \quad \delta r_{\rm a} \to \frac{\delta r_{\rm a}}{2}, \quad r_{\rm a} \to -r_{\rm a},$$

one can find that his equation 45 is identical to our equation (62).

C.6 Full propagation of rf sidebands from input to the AS port

Similarly to the carrier field, the Michelson reflectivity and transmissivity can be written as

$$\begin{aligned} r_{\rm M}^{\rm (sb)} &= r_{\rm com}^{\rm (sb)} \cos\left(\frac{l_{\rm sch}}{c}\left(\omega_{\rm m}+\omega\right)\right) - i r_{\rm diff}^{\rm (sb)} \sin\left(\frac{l_{\rm sch}}{c}\left(\omega_{\rm m}+\omega\right)\right), \\ t_{\rm M}^{\rm (sb)} &= i r_{\rm com}^{\rm (sb)} \sin\left(\frac{l_{\rm sch}}{c}\left(\omega_{\rm m}+\omega\right)\right) - r_{\rm diff}^{\rm (sb)} \cos\left(\frac{l_{\rm sch}}{c}\left(\omega_{\rm m}+\omega\right)\right). \end{aligned} \tag{63}$$

where $\omega_{\rm m}$ is the rf modulation frequency and $r_{\rm com}^{\rm (sb)}$ and $r_{\rm diff}^{\rm (sb)}$ are the common and differential reflectivity of the arm cavities for the rf sidebands, defined as

$$r_{\rm com}^{\rm (sb)} = \hat{r_{\rm a}}, \quad r_{\rm diff}^{\rm (sb)} = 2i\hat{r_{\rm a}}'\frac{\omega L}{c}\frac{\delta T_{\rm i}}{T_{\rm i}}. \tag{64}$$

With δT_i being the difference in the ITM reflectivity. It is defined by $\delta T_{\rm i} = (T_{\rm ix} - T_{\rm iy})/2$. So we now use $\delta T_{\rm i}$ instead of $(\delta r_{\rm a}, \delta\omega_{\rm c}, \epsilon)$ for convenience.

Since the AS field can be written as

$$\frac{E_{\rm as}^{\rm (sb)}}{E_{\rm in}^{\rm (sb)}} = \frac{t_{\rm p} t_{\rm s} t_{\rm M}^{\rm (sb)}}{1 + \left(r_{\rm p}+r_{\rm s}\right) r_{\rm M}^{\rm (sb)} + r_{\rm p} r_{\rm s} \hat{r_{\rm a}}^2}, \tag{65}$$

one can rewrite it with the above equations plugged,

$$\frac{E_{\rm as}^{\rm (sb)}}{E_{\rm in}^{\rm (sb)}} = g_{\rm sb} t_{\rm sb} + s_{\rm c} t_{\rm p} t_{\rm s} \hat{r_{\rm a}} \left(\frac{l_{\rm sch}\omega_{\rm c}}{c} - \frac{2L\omega_{\rm c}}{c}\frac{\delta T_{\rm i}}{T_{\rm i}}\frac{\hat{r_{\rm a}}'}{\hat{r_{\rm a}}}\right) \frac{\cos\phi_{\rm sch} + \left(r_{\rm p}+r_{\rm s}\right)\hat{r_{\rm a}} + r_{\rm p} r_{\rm s} \hat{r_{\rm a}}^2 \cos\phi_{\rm sch}}{\left(1 + \left(r_{\rm p}+r_{\rm s}\right)\hat{r_{\rm a}}\cos\phi_{\rm sch} + r_{\rm p} r_{\rm s} \hat{r_{\rm a}}^2\right)^2}. \tag{66}$$

D Numerical parameters

symbol	description	value
$T_{\rm i}$	ITM power transmissivity	0.0140
$\lambda_{\rm i}$	ITM loss on the HR surface	0
$t_{\rm i}$	ITM amplitude transmissivity or $\sqrt{T_{\rm i}}$	
$r_{\rm i}$	ITM amplitude reflectivity or $\sqrt{1-T_{\rm i}-\lambda_{\rm i}}$	
$T_{\rm e}$	ETM power trasmissivity	50e-6
$\lambda_{\rm e}$	ETM loss on the HR surface	0
$t_{\rm e}$	ETM amplitude transmissivity or $\sqrt{T_{\rm e}}$	
$r_{\rm e}$	ETM amplitude reflectivity or $\sqrt{1-T_{\rm e}-\lambda_{\rm e}}$	
$T_{\rm p}$	PRM power trasmissivity	0.031
$\lambda_{\rm p}$	PRM loss on the HR surface	0
$t_{\rm p}$	PRM amplitude transmissivity or $\sqrt{T_{\rm p}}$	
$r_{\rm p}$	PRM amplitude reflectivity or $\sqrt{1-T_{\rm p}-\lambda_{\rm p}}$	
$T_{\rm s}$	SRM power trasmissivity	0.37
$\lambda_{\rm s}$	SRM loss on the HR surface	0
$t_{\rm s}$	SRM amplitude transmissivity or $\sqrt{T_{\rm s}}$	
$r_{\rm s}$	SRM amplitude reflectivity or $\sqrt{1-T_{\rm s}-\lambda_{\rm s}}$	
	optical distances	
$L_{\rm arm}$	arm length (both X and Y)	3994.5 m
$l_{\rm sch}$	Schnupp asymmetry	0.08 m
$l_{\rm p}$	Power recycling cavity length	57.65 m
$l_{\rm s}$	Signal recycling cavity length	56.0 m
L_ϵ	DARM offset	20 pm
	Laser property	
$P_{\rm in}$	input laser power	1 W
f_1	modulation frequency of the first rf sideband	9099451 Hz
f_2	modulation frequency of the second rf sideband	45497255 Hz
Γ_1	modulation depth of the f_1 rf sideband	0.1 rad
Γ_2	modulation depth of the f_2 rf sideband	0.1 rad

Table 3: Summary of the numerical parameters for the length responses. No losses are included for simplicity

symbol	description	value
	ITM properties	
δT_i	difference in ITM power transmissivity	100 ppm
λ_i	ITM loss on the HR surface	0
T_ix	ITMX power transmissivity $T_\mathrm{i} + \delta T_\mathrm{i}$	0.141
T_iy	ITMY power transmissivity $T_\mathrm{i} - \delta T_\mathrm{i}$	0.139
t_ix	ITMX amplitude transmissivity or $\sqrt{T_\mathrm{ix}}$	
t_iy	ITMY amplitude transmissivity or $\sqrt{T_\mathrm{iy}}$	
r_ix	ITMX amplitude reflectivity or $\sqrt{1 - T_\mathrm{i} - \delta T_\mathrm{i}}$	
r_iy	ITMY amplitude reflectivity or $\sqrt{1 - T_\mathrm{i} + \delta T_\mathrm{i}}$	
	ETM properties	
λ_e	ETM loss on the HR surface	30 ppm
$\delta\lambda_\mathrm{e}$	ETM differential loss on the HR surface	-20 ppm
r_ex	ETMX amplitude reflectivity or $\sqrt{1 - T_\mathrm{e} - \lambda_\mathrm{e} - \delta\lambda_\mathrm{e}}$	
r_ey	ETMY amplitude reflectivity or $\sqrt{1 - T_\mathrm{e} - \lambda_\mathrm{e} + \delta\lambda_\mathrm{e}}$	
	Arm cavity properties	
$\omega_\mathrm{c}^{(\mathrm{xarm})}/(2\pi)$	X arm cavity pole	42.5842 Hz
$\omega_\mathrm{c}^{(\mathrm{yarm})}/(2\pi)$	Y arm cavity pole	42.0980 Hz
$\delta\omega_\mathrm{c}/(2\pi)$	Difference in the cavity pole frequency or $(\omega_\mathrm{c}^{(\mathrm{xarm})} - \omega_\mathrm{c}^{(\mathrm{yarm})})/(4\pi)$	0.24313 Hz
$r_\mathrm{a}^{(\mathrm{xarm})}$	X arm reflectivity for the carrier light	0.99159
$r_\mathrm{a}^{(\mathrm{yarm})}$	Y arm reflectivity for the carrier light	0.985812
δr_a	Difference in arm reflectivity or $(r_\mathrm{a}^{(\mathrm{xarm})} - r_\mathrm{a}^{(\mathrm{xarm})})/2$	0.002886

Table 4: Summary of the numerical parameters for the laser noise couplings. Loss is added to ETMs. ITMs have different reflectivity. The rest of parameters are unchanged from table 3

.

References

[1] K. Izumi and D. Sigg,"Frequency response of the aLIGO interferometer: part 1", LIGO-T1500461(2015)
https://dcc.ligo.org/LIGO-T1500325

[2] Daniel Sigg, "Frequency Response of the LIGO Interferometer", LIGO-T970084 (1997)
https://dcc.ligo.org/LIGO-T970084

[3] Peter Fritschel et al.,"Readout and control of a power-recycled interferometric gravitational-wave antenna", Applied Optics, 40 28 (2001)

[4] Martin Regehr, "Signal Extraction and Control for an Interferometric Gravitational Wave Detector", Thesis, Caltech (1995)

[5] Nicolas Smith-Lefebvre, "Techniques for Improving the Readout Sensitivity of Gravitational Wave Antennae", Thesis, Massachusetts Institute of Technology (2012)
https://dcc.ligo.org/LIGO-P1200052

[6] Koji Arai et al., "Output Mode Cleaner (OMC) Design", LIGO-T1000276-v5 (2013)
https://dcc.ligo.org/LIGO-T1000276

[7] Jordan Camp, "Frequency, Intensity and Oscillator Noise in the LIGO", LIGO-T960019 (1996)
https://dcc.ligo.org/LIGO-T960019

[8] K. Izumi, D. Sigg and K. Kawabe, "Frequency response of the aLIGO interferometer: part 3", LIGO-T1500559(2015)
https://dcc.ligo.org/LIGO-T1500325